RSC Advances

PAPER

View Article Online
View Journal | View Issue

Cite this: *RSC Adv.*, 2018, **8**, 12029

Bio-inspired self-assembly of waxberry-like core-shell SiO_2@TiO_2 nanoparticles towards antiglare coatings

Mingli Yu,[ab] Aihua Sun, *[b] Chengyi Chu,[b] Tao Chen,[ab] Chengbing Yu,[a] Biao Wang,[b] Jianjun Guo[b] and Gaojie Xu[b]

Received 25th January 2018
Accepted 13th March 2018

DOI: 10.1039/c8ra00775f

rsc.li/rsc-advances

Waxberry-like core–shell SiO_2@TiO_2 nanoparticles were prepared by liquid-phase deposition (LPD) method. The dip-coating self-assembly of waxberry-like core–shell SiO_2@TiO_2 nanoparticles has been used to fabricate coatings with excellent antiglare properties in the large angle and wide wavelength range. The field emission scanning electron microscopy (SEM) and transmission electron microscopy (TEM) measurements showed that the surface of SiO_2 nanoparticles were coated by titania as a shell with controllable and uniform thickness. The ultraviolet visible near-infrared spectrophotometer (UV-Vis-NIR) results indicate that the maximum transmittance of the antiglare coating is up to 95.80% in the visible band, whereas that of the pure glass substrate is only 92.10%. The scattering and haze of the films have been measured to show that such specifically structured coatings exhibited good antiglare properties in the large angle and wide wavelength range.

Introduction

Glare has been one of the most important reasons for night traffic accidents and visual fatigue. With the appearance and development of high-brightness synchrotron radiation sources, light pollution has become an increasingly serious problem. The most effective solution is to use high transparency coatings to realize an antireflective and antiglare purpose. An antireflective and antiglare film comprises three major components: light-scattering particles, binding resin, and substrates.[1–5] Specifically structured films have been attracting much attention in application of antireflective and antiglare technologies to lower the intensity of the glare by reducing the light reflection.[1,6–18] Various approaches have been developed to construct specifically structured functional films including hard or soft template method, electrochemical deposition, phase separation of polymers, domain-selective treatment by etching or lithography, hydrothermal reaction and self-assembly. Two schemes have been developed to reduce the light reflection: (1) make an antireflective and antiglare coating with roughened surface to scatter the undesirable light; (2) choose low reflective index film material to reduce the light reflection by destructive interference.[1,13–16,19,20]

Some studies have revealed that the glare can be avoided by controlling the ratio of light-scattering particles to the binding resin, the difference in refractive indices of the light-scattering particles and the binding resin, the diameter of the light-scattering particles and the thickness of antiglare coatings. Kawahara *et al.* added inorganic particles, such as silica, alumna, titania, *etc.*, to a UV-curable binder to form antiglare coatings on triacetate cellulose (TAC), which finds applications in LCD.[21] Kahp Y. Suh *et al.* have fabricated a polyurethane acrylate (PUA) sheet by partial photo polymerization and dry etching, which have functions of antireflection and antifogging.[22] However, these antiglare coatings with suspended particles can reduce the glare and light reflection but often cause a significant weakness in image resolution and readability because of the use of organic polymer.[13,14] The light diffusion effect is relatively unsatisfactory due to the sacrifice of clarity, contrast, and resolution of transmitted images. Additionally, most of the methods require complicated fabrication processes and expensive equipment.[23] Low refractive-index films or vary refractive-index coatings by adding pure inorganic nanoparticles may solve the above problems.[24] It is known that SiO_2 has excellent properties such as low reflective index, low dielectric constant, chemical stability and corrosion-resistant property.[25–27] Otherwise, TiO_2 has been widely applied in many different kind of coating by compounding with other material, such as SiO_2 and Al_2O_3, as an important functional coating inorganic material. Because of high refractive index of TiO_2, the film coated TiO_2 has broadband antireflection properties to be applied to different kinds of functional coating, which make it extremely attractive for practical applications in

[a]*Department of Polymer Materials, School of Materials Science and Engineering, Shanghai University, Nanchen Road 333, Shanghai 200444, China*

[b]*Key Laboratory of Additive Manufacturing Material of Zhejiang Province, Department of Functional Materials and Nano-Devices, Ningbo Institute of Materials Technology & Engineering, Chinese Academy of Sciences, 1219 Zhongguan West Road, Ningbo 315201, China. E-mail: sunaihua@nimte.ac.cn*

optical devices, display devices, and photovoltaic cells.[28,29] For these excellent performance, there is broad application prospect to manufacture antiglare film with SiO_2 and TiO_2. Wang *et al.* have prepared a SiO_2/TiO_2 antireflective coatings with self-cleaning properties *via* sol–gel process and calcination process.[30] Besides, researchers have designed various projects to improve antiglare property in the large angle and wide wavelength range. Noboru Yamada *et al.* have characterized antireflective moth-eye films placed on top of crystalline silicon photovoltaic modules by indoor and outdoor experiments and examined improvements in conversion efficiency.[31] The moth's eye structure have the uniform bulges on the surface that show excellent antiglare property in the large angle and wide wavelength range.[32,33] Therefore, there is urgent need to develop an easy method for preparing bio-inspired structured inorganic nanoparticles to fabricate antiglare films with good antiglare property in the large angle and wide wavelength range.

In this paper, we have reported a novel waxberry-like core–shell nanoparticle that SiO_2 nanoparticle as core with nanosized titania as shell obtained by a liquid-phase deposition (LPD) method.[34] The dip-coating assembly has been used for constructing films with waxberry-like core–shell $SiO_2@TiO_2$ nanoparticles. Exciting antiglare property was achieved on this film by controlling the way in which the light can propagate (Fig. 1). It is distinct that the surface of the waxberry-like core–shell $SiO_2@TiO_2$ nanoparticles have many small inhomogeneous projections. When the incident light irradiating on the surface of the waxberry-like core–shell nanoparticles, the incident light could be scattered in all direction by the microscopic inhomogeneous projections. At the same time, this specific waxberry-like core–shell structure could form gradual refractive index because SiO_2 and TiO_2 have different refractive index. Antiglare performance from gradual refractive index is based on the principle of light refraction. By building antiglare film with refractive index gradient, the reflected light is gradually reflected to other directions to reduce the intensity of reflected light entering the eyes to achieve antiglare property. Besides, through further adjustment of film thickness and refraction rate, the reflected light could interfere destructively to weaken the reflected light flux entering the eyes, achieving better antiglare performance.[16] When internal lights pass through the coating, part of collimated light is scattered to the side of the display because of the waxberry-like core–shell nanoparticles, to improve internal light's scattering intensity and background luminance. The excellent coating could ensure the definition of images with wide angular range that users could feel comfortable. External light passing through the coating, it will be scattered by the raised shell of the waxberry-like core–shell nanoparticles, avoiding contrasted light into the eyes to eliminate the glare. Due to the scattering of external light, antireflective (AR) and antiglare (AG) technologies are usually applied in liquid crystal displays or touch panels to prevent the deterioration of visibility by reflective light.

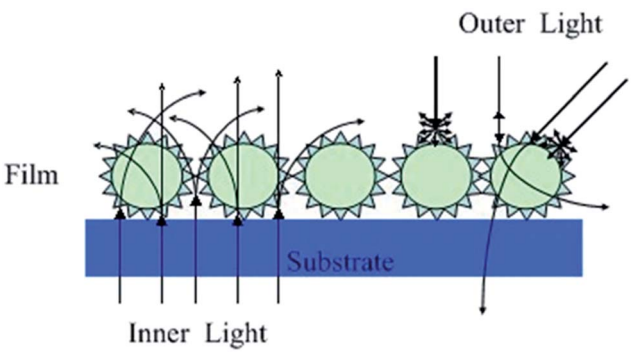

Fig. 1 Antiglare mechanism of coating with waxberry-like core–shell nanoparticles.

Experimental section

Materials

Tetraethoxysilane (TEOS, AR), titanium tetraisopropanolate (TTIP, AR), ethanol (AR), $NH_3 \cdot H_2O$ (25%, AR), polyelectrolyte polyallylamine hydrochoride (PAH, $M_w = 70\,000$, Aldrich) were purchased from Sinopharm Chemical Reagent Company (Shanghai, China). All chemicals were used as received without further purification. The water used in this work was deionized (DI) water from a Millipore-Q purification system (Millipore, USA) of resistivity 18.2 MΩ cm.

Preparation of $SiO_2@TiO_2$ nanoparticles and antiglare coating

The silica was prepared by stÖber method.[35] Modification of the surface of silica nanoparticles using polyelectrolyte polyallylamine hydrochoride by a layer-by-layer technique (Fig. 2) as described elsewhere.[36] In our previous works, the difference in the concentration of $(NH_4)_2TiF_6$ can be easily used to control of the thickness of TiO_2 shells. Meanwhile, the TiO_2 shell had a uniform cross-section over the entire surface of SiO_2 core and the shell thickness was increased with increasing the $(NH_4)_2TiF_6$ content.[34] The specific works are as follows, the PAH-functionalized silica nanoparticles were dispersed in 80 mL deionized water. Then, a given amount of 0.1 mol L^{-1} $(NH_4)_2TiF_6$ solution was added to the dispersion followed by ultrasonication for 1 h and adjustment of pH to 2.8 using a 0.2 M HCI solution. Finally, a 0.6 M H_3BO_3 acid solution was obtained by dropping titanium isopropoxide (TIPT)/ethanol solution into the SiO_2 sol which having prepared above under mechanical stirring. All nanoparticles were collected by centrifugation, washed with deionized water, and dried at 60 °C for 12 h. The waxberry-like core–shell $SiO_2@TiO_2$ antiglare coatings were prepared as follows: a mass of uniformly waxberry-like core–shell $SiO_2@TiO_2$ was dispersed into ethanol; then a dip-coating self-assembly process was undertake at the rate of 20

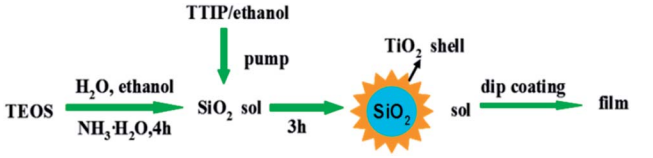

Fig. 2 Schematic illustration of particulate coating from self-assembly of waxberry-like core–shell $SiO_2@TiO_2$ nanoparticles.

cm min^{-1} to produce uniform coatings on the surface of the glasses at 25 °C.

Characterization

A field emission scanning electron microscopy (SEM; S4800; Hitachi, Japan) was used to observe the morphology of the TiO_2 on the surface of silica nanoparticles. Fourier transform infrared spectroscopy (FTIR; Nicolet 6700; American) of the core–shell nanoparticle was obtained in the region 400–4000 cm^{-1}. The thickness of the shell was investigated by Transmission Electron Microscope (TEM; Tecnai F20; EI, America). The crystalline structure of the core–shell nanoparticle was characterized using TEM selected-area electron diffraction (SAED). The haze of the coating was measured by a haze meter (WGT-S, Shanghai Chenguang Instrument CO. LTD). The transmission and reflection of the coating were measured by an ultraviolet visible near-infrared spectrophotometer (UV-Vis-NIR; Lambda 950; Perkin Elmer, America). The incident angle dependence reflectivity were tested *via* the spectroscopic ellipsometry measurements (M-2000DI, J.A.Woollam Co, Inc, USA). The photographs of the films were recorded with a Canon EOS 500D digital camera.

Results and discussion

Fig. 3 shows SEM and TEM images of 120 nm waxberry-like core–shell SiO_2@TiO_2 nanoparticles and selective area electron diffraction (SAED) of core–shell SiO_2@TiO_2 nanoparticles. As showed in Fig. 3a, the waxberry-like core–shell nanoparticles exhibit essentially the same size and very good dispersibility in the SEM images. Furthermore, approximate 10 nm thick TiO_2 shell layers can be observed on the surface of the core–shell SiO_2@TiO_2 nanoparticles in the SEM and TEM images (Fig. 3b and d). The continuous and dotty rings in selective area electron diffraction in inset of Fig. 3d indicate the existence of tiny and relatively larger crystals respectively, verifies the polycrystalline feature of the TiO_2 shell. Herein, through TEM and SAED analysis, there is no evidence for oxide compounds or crystals except TiO_2.

Fig. 4 shows FTIR spectra of SiO_2 nanoparticles and core–shell SiO_2@TiO_2 nanoparticles by LPD method in the region 400–4000 cm^{-1}. The core–shell nanoparticles can be observed in the broad absorption bands in 470–798 cm^{-1}, which is corresponding to Ti–O–Ti network; and 800–1100 cm^{-1} corresponding to Si–O–Ti and Si–O–Si network. The slightly increased absorption inside the circle at 470–798 cm^{-1} showed that there is Ti–O–Ti stretch vibration absorption in the core–shell SiO_2@TiO_2 nanoparticles. It is obvious that the absorption peak at 954 cm^{-1} moves to 938 cm^{-1}. The shift indicates the existence of Si–O–Ti asymmetric stretching vibration absorption. The peaks at 3192 cm^{-1} and 1403 cm^{-1} indicated that Ti–OH groups exist in the core–shell SiO_2@TiO_2 nanoparticles. From these results, it can be concluded that the obtained nanoparticles have core–shell structure composed of SiO_2 and TiO_2.

Fig. 5 shows SEM images of SiO_2 nanoparticles and SiO_2 nanoparticles with homogeneous TiO_2 shell. In Fig. 5a and b, 120 nm SiO_2 nanoparticles are coated on the surface of the glass and packed tightly together. As is seen from Fig. 5c and d, the 120 nm waxberry-like core–shell SiO_2@TiO_2 nanoparticles synthesized in this work possessed uniform size and surface roughness. The film was found that the surface of the film is relatively flat and 120 nm waxberry-like core–shell SiO_2@TiO_2 nanoparticles are arranged in an orderly manner. The diameter of waxberry-like core–shell SiO_2@TiO_2 nanoparticles are about 40 nm in Fig. 5e. As clearly seen from Fig. 5e and f, the 40 nm waxberry-like core–shell nanoparticles became tightly packed to form aggregation easily. It is difficult to realize effective control of the path of light propagation. In Fig. 5g and h, 600 nm waxberry-like core–shell SiO_2@TiO_2 nanoparticles distribution tends to be evidently uneven. It can be observed that large particles might be hard to adhere to the surface of the glass to constitute close-packed structure. Clearly, more 120 nm waxberry-like core–shell SiO_2@TiO_2 nanoparticles are adsorbed on the pure glass surface to build compact films, which is believed to be advantageous for forming rougher surface. The

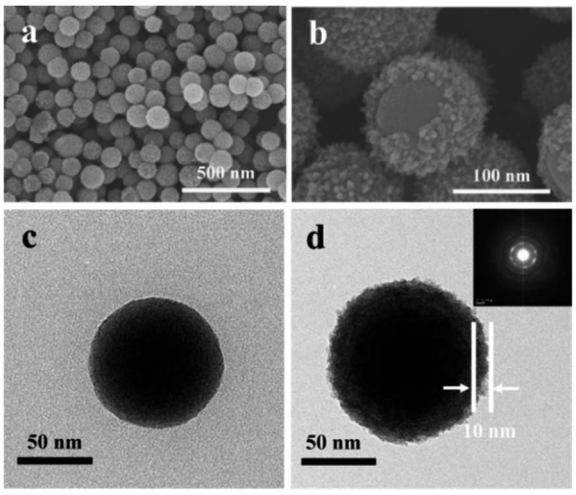

Fig. 3 SEM image of (a), (b) SiO_2@TiO_2 and TEM image of (c) SiO_2 and (d) SiO_2@TiO_2 inset is the SAED of SiO_2@TiO_2.

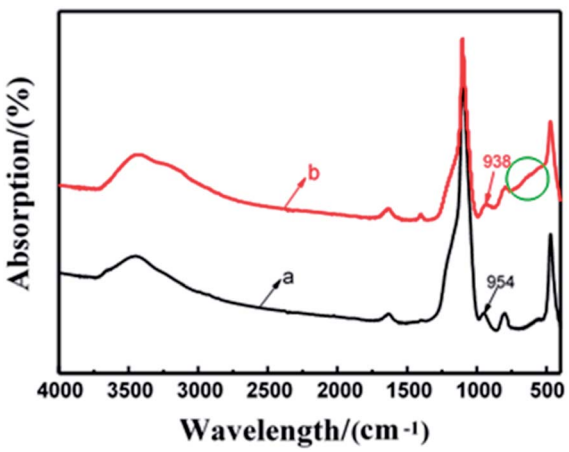

Fig. 4 FTIR spectra of (a) SiO_2 and (b) SiO_2@TiO_2.

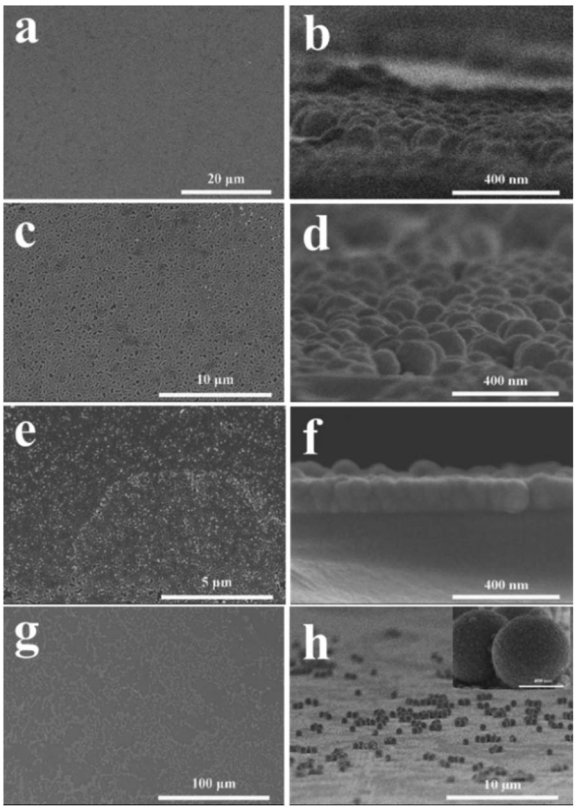

Fig. 5 SEM images of LPD method (a) 120 nm SiO_2; (c) 120 nm SiO_2@TiO_2; (e) 40 nm SiO_2@TiO_2; (g) 600 nm SiO_2@TiO_2. (b, d, f, h) Side view of a, c, e, g, respectively.

surface roughness is believed to affect the transmittance and antiglare property of coating, which is discussed below in detail.

Direct reflection of film with coating SiO_2 nanoparticles or different size core–shell SiO_2@TiO_2 nanoparticles (by LPD method) under the condition of vertical incidence was shown in Fig. 6. It is obvious that specular reflectance of the glass after coating is lower than that of the glass without coating. As a result, all films that the core–shell SiO_2@TiO_2 nanoparticles are coated on the surface of the glasses exhibited good antiglare property compared with the pure glass. Of those, the direct reflection of the film with adding 120 nm SiO_2 nanoparticles or waxberry-like core–shell SiO_2@TiO_2 nanoparticles is lower than the other kinds of films. It can be observed that the film coated 120 nm waxberry-like core–shell SiO_2@TiO_2 nanoparticles possess weaker reflectance in broader spectral range in comparison to the film coated 120 nm SiO_2 nanoparticles. The waxberry-like core–shell SiO_2@TiO_2 nanoparticles have many small inhomogeneous projections on the surface. It is these microscopic inhomogeneous projections that interact with the incident light in a specific way. When the incident light interacts with the rough surface as if the surface has a gradient refractive index, light rays tend to bend progressively to scatter in other directions to weaken the intensity of reflected light.[16] This could help explain that the surface roughness of waxberry-like core–shell SiO_2@TiO_2 nanoparticles is greater than surface roughness of SiO_2 nanoparticles to effectively reduce the reflection of internal light and external light. Based on the above, the film coated 120 nm waxberry-like core–shell SiO_2@TiO_2 nanoparticle has the best antireflective and antiglare performance.

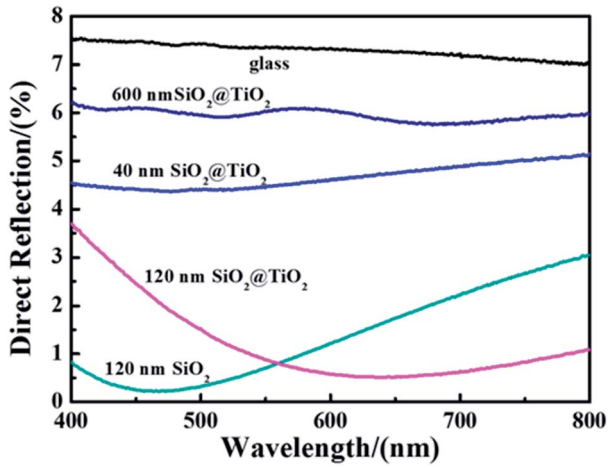

Fig. 6 Direct reflection of different coating.

Antiglare property of the film is closely related to specular reflectance and haze. The proper haze is beneficial to reduce the intensity of glare into the eyes and improve the definition of the images. Too low haze will cause strong reflection and poor antiglare performance. Too high haze will lead to high intensity of light scattering to weaken contract, brightness and sharpness of images. As shown in Table 1, the transmittance and the haze of the 120 nm waxberry-like core–shell SiO_2@TiO_2 nanoparticle film are 95.80% and 2.66%, respectively. These results would give some indication that the specifically structured coatings show the antiglare property in the large angular range.

The scattering of film with different 120 nm nanoparticles under the condition of verticals incidence was shown in Fig. 7. The scattering of the film with 120 nm waxberry-like core–shell SiO_2@TiO_2 nanoparticles was up to 5.5%. It indicates that waxberry-like core–shell SiO_2@TiO_2 nanoparticles on the surface are better at changing the path of light propagation, avoiding strong light into naked eyes, to increase antiglare performance. Besides, the scatterance of the waxberry-like core–shell nanoparticles is higher because of excellent refractive of the waxberry-like core–shell nanoparticles' TiO_2 shell, in favour of improving antiglare property.

The p-Reflection of the pure glass and the antiglare coating with 120 nm nanoparticles in wide angular range is shown in Fig. 8. Under the same observation angles, the p-Reflection of the glass with waxberry-like core–shell SiO_2@TiO_2

Table 1 The transmittance and haze of different samples

	Sample	Transmittance (%)	Haze (%)
a	Glass (K9)	92.10	0.21
b	120 nm SiO_2	97.41	0.43
c	120 nm SiO_2@TiO_2	95.80	2.66
d	40 nm SiO_2@TiO_2	93.73	0.71
e	600 nm SiO_2@TiO_2	91.16	22.32

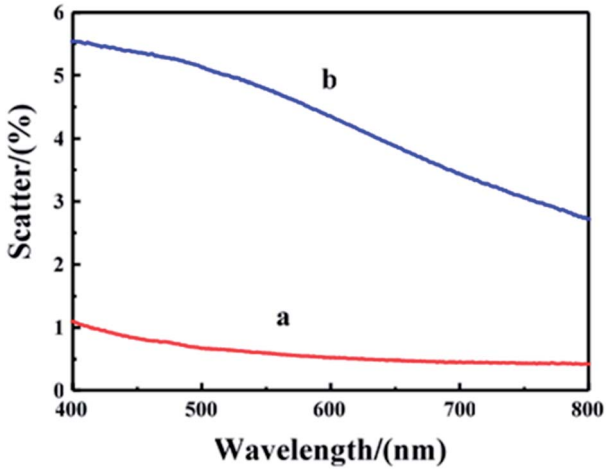

Fig. 7 Scattering of (a) 120 nm SiO_2 and (b) 120 nm SiO_2@TiO_2.

nanoparticles coating (GST) is lower than it of the pure glass (G) and the glass substrate with SiO_2 nanoparticles coatings (GS). The result indicated that GST possesses better antireflective and antiglare property. Similarly this means that the TiO_2 shell of the film surface is able to effectively change the way of light propagation. When observation angle is less than 60°, the p-Reflection of GST is close to 0, indicating that GST has excellent antiglare property to reduce intensity reflection in the range from 0° to 120°. When observation angle rises to 70°, the most p-Reflection of GST is about 8.7%, with good antiglare property. When observation angular reaches up to 80°, the minimum of p-Reflection of GST is over 39%, with no antiglare property.

As shown in Fig. 9, reflected light of the film with coating 120 nm waxberry-like core–shell SiO_2@TiO_2 nanoparticles is amaranthine. And we can get a clear image about the words behind the glass. The TiO_2 shell with high refractive index, coated on the surface of the waxberry-like core–shell nanoparticles, can evidently enhance luminance to further improvement in antiglare performance. That may be because the special waxberry-like particulate coatings with core–shell

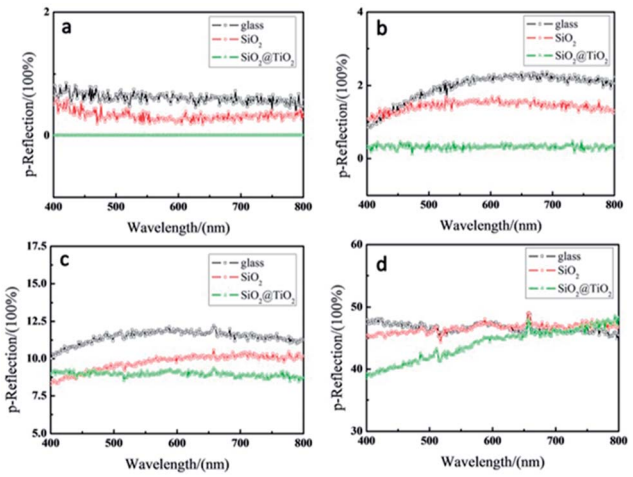

Fig. 8 Reflection of antiglare coating under different observation angle of (a) 50°, (b) 60°, (c) 70°, (d) 80°.

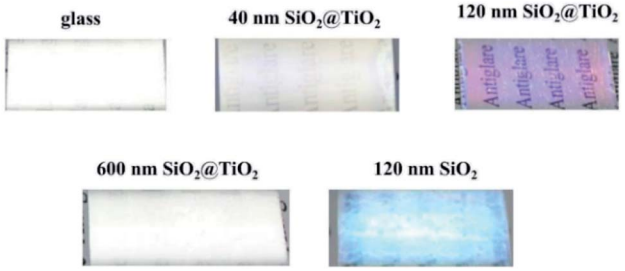

Fig. 9 Photographs of different coating.

nanoparticles are as good as to show high transparency due to change propagation of light, as well as the appropriate void fraction and surface roughness of 120 nm waxberry-like core–shell SiO_2@TiO_2 coating is in favor of the antiglare behaviour.

Conclusions

Waxberry-like core–shell SiO_2@TiO_2 nanoparticles were prepared *via* a liquid-phase deposition method. Furthermore, the dip-coating self-assembly of waxberry-like core–shell SiO_2@TiO_2 nanoparticle has been used to construct antiglare coatings. The ultraviolet visible near-infrared spectrophotometer result indicates that the maximum transmittance of the antiglare coating is up to 95.80% in the visible band, whereas that of the pure glass substrate is only 92.10%. This specifically structured coatings with large surface roughness have exhibited excellent antiglare property in the large angle and wide wavelength range. Besides, this method to fabricate antiglare coatings with pure inorganic nanoparticle is commercial and environmental-friendly to avoid complicated fabrication processes and expensive equipment. Therefore, the current work would provide a simple, versatile way and a blue print for designing this special structure with waxberry-like core–shell nanoparticles to fabricate antiglare coatings with good antiglare property in the large angle and wide wavelength range.

Conflicts of interest

There are no conflicts to declare.

Acknowledgements

This research is funded by National Natural Science Foundation of China (Grant no.11404347, 11574331). We also express our gratitude to the aided program for Science and Technology Innovative Research Team of Ningbo Municipality (2015B11002, 2016B10005) and the Science and Technology Support Project of Jiangsu Provincial Sci. & Tech. Department (BE2013082).

Notes and references

1 B. T. Liu and Y. T. Teng, *J. Colloid Interface Sci.*, 2010, **350**, 421–426.
2 H. Jiang, K. Yu and Y. Wang, *Opt. Lett.*, 2007, **32**, 575–577.

3 P. Eiamchai, P. Chindaudom, M. Horprathum, V. Patthanasettakul and P. Limsuwan, *Mater. Des.*, 2009, **30**, 3428–3435.
4 B. T. Liu and W. D. Yeh, *Colloids Surf., A*, 2010, **356**, 145–149.
5 P. Eiamchai, M. Horprathum, V. Patthanasettakul, P. Limnonthakul, N. Nuntawong, P. Limsuwan and P. Chindaudom, *Mater. Des.*, 2010, **31**, 3151–3158.
6 P. I. Stavroulakis, S. A. Boden, T. Johnson and D. M. Bagnall, *Opt. Express*, 2013, **21**, 1–11.
7 B. G. Prevo, Y. Hwang and O. D. Velev, *Chem. Mater.*, 2005, **17**, 3642–3651.
8 Z. Wu, J. Walish, A. Nolte, L. Zhai, R. E. Cohen and M. F. Rubner, *Adv. Mater.*, 2006, **18**, 2699–2702.
9 K. C. Krogman, T. Druffel and M. K. Sunkara, *Nanotechnology*, 2005, **16**, S338.
10 B. T. Liu, Y. T. Teng, R. H. Lee, W. C. Liaw and C. H. Hsieh, *Colloids Surf., A*, 2011, **389**, 138–143.
11 X. Liu and J. He, *J. Colloid Interface Sci.*, 2007, **314**, 341–345.
12 J. C. Chien, T. W. Lai, B. P. Wang and H. C. Chen, *US pat.* 6852376, 2005.
13 D. Tulli, S. D. Hart, P. Mazumder, A. Carrilero, L. Tian, K. W. Koch, R. Yongsunthon, G. A. Piech and V. Pruneri, *ACS Appl. Mater. Interfaces*, 2014, **6**, 11198–11203.
14 S. Takei, G. Murakami, Y. Mori, T. Ichikawa, A. Sekiguchi, T. Obata, Y. Yokoyama, W. Mizuno, J. Sumioka and Y. Horita, *J. Micro/Nanolithogr., MEMS, MOEMS*, 2013, **12**, 031113.
15 C. C. Chang, C. M. Chen, F. H. Hwang, C. C. Chen and L. P. Cheng, *J. Coat. Technol. Res.*, 2012, **9**, 561–568.
16 H. K. Raut, V. A. Ganesh, A. S. Nair and S. Ramakrishna, *Energy Environ. Sci.*, 2011, **4**, 3779–3804.
17 K. Manabe, M. Matsuda, C. Nakamura, K. Takahashi, K. H. Kyung and S. Shiratori, *Chem. Mater.*, 2017, **29**, 4745–4753.
18 S. B. Khan, H. Wu, Z. Fei, S. Ning and Z. Zhang, *Nanoscale*, 2017, **9**, 11047–11054.
19 A. Sakai and M. Yamahara, *US pat.* 6992827, 2006.
20 J. Dobrowolski, D. Poitras, P. Ma, H. Vakil and M. Acree, *Appl. Opt.*, 2002, **41**, 3075–3083.
21 S. Kawahara and N. Takahashi, *US pat.* 6970213, 2005.
22 D. Tahk, T. I. Kim, H. Yoon, M. Choi, K. Shin and K. Y. Suh, *Langmuir*, 2010, **26**, 2240–2243.
23 J. Wang, C. Zhang, C. Yang, C. Zhang, M. Wang, J. Zhang and Y. Xu, *ACS Appl. Mater. Interfaces*, 2017, **9**, 5468–5476.
24 Z. Ji, L. Bao, H. Wang and R. Chen, *Mater. Lett.*, 2017, **207**, 21–24.
25 H. Zhang, C. Lou, X. Huang, X. Yu, H. Yang and D. Pribat, *Appl. Phys. Lett.*, 2017, **111**, 201602.
26 B. Xia, J. Luo, Y. Li, B. Yang and S. Zhang, *RSC Adv.*, 2017, **7**, 26834–26838.
27 L. Ai, J. Zhang, X. Li, Y. Lu and W. Song, *ACS Appl. Mater. Interfaces*, 2018, **10**, 4993–4999.
28 B. Jin, J. He, L. Yao, Y. Zhang and J. Li, *ACS Appl. Mater. Interfaces*, 2017, **9**, 17466–17475.
29 L. Q. Ye, Q. H. Zhang, Y. L. Zhang, X. X. Zhang and B. Jiang, *Inorg. Mater.*, 2012, **27**, 871–875.
30 J. W. Wang, Y. C. Bai, W. Yao, H. N. Wang and R. Y. Chen, *Inorg. Mater.*, 2011, **7**, 018.
31 N. Yamada, T. Ijiro, E. Okamoto, K. Hayashi and H. Masuda, *Opt. Express*, 2011, **19**, A118–A125.
32 M. S. Mirotznik, B. L. Good, P. Ransom, D. Wikner and J. N. Mait, *IEEE Trans. Antennas Propag.*, 2010, **58**, 2969–2980.
33 K. Forberich, G. Dennler, M. C. Scharber, K. Hingerl, T. Fromherz and C. J. Brabec, *Thin Solid Films*, 2008, **516**, 7167–7170.
34 H. Huang, A. Sun, J. Zhang, B. Wang, C. Chu, Y. Li and G. Xu, *Mater. Lett.*, 2013, **110**, 260–263.
35 W. Stöber, A. Fink and E. Bohn, *J. Colloid Interface Sci.*, 1968, **26**, 62–69.
36 H. Strohm and P. Löbmann, *Chem. Mater.*, 2005, **17**, 6772–6780.